buildings

MDPI

Article

Size Effect Analysis on Shear Mechanical Behavior of Prestressed RAC Beams Under Dynamic Loading

Chunyang Liu [1,2,*], Xintong Li [3], Bin He [1,2], Wusiman Naibi [1,2], Fahad Ali [4] and Zhenyun Tang [5]

[1] School of Civil Engineering, Kashi University, Kashi 844000, China
[2] Xinjiang Key Laboratory of Engineering Materials and Structural Safety, Kashi 844000, China
[3] Department of Civil Engineering, Shandong Jianzhu University, Jinan 250101, China
[4] Department of Geology, Bacha Khan University Charsada, Charsadda 24450, Pakistan
[5] The Key Laboratory of Urban Security and Disaster Engineering of the Ministry of Education, Beijing University of Technology, Beijing 100124, China
* Correspondence: liucy2011@sdjzu.edu.cn

Abstract

To reveal the evolution laws of shear mechanical behavior and size effect of prestressed Recycled Aggregate Concrete (RAC) beams under dynamic loading conditions, a three-dimensional five-phase meso-scale numerical model was established based on the ABAQUS2020 software. The bond–slip behavior between steel bars and concrete was considered, and prestress was applied using the temperature cooling method. The effects of prestress level, cross-sectional size and strain rate on failure modes, load–displacement curves, ultimate shear capacity and nominal shear strength were systematically investigated. The results show that increasing the prestress level can significantly restrain the initiation and propagation of diagonal cracks, reduce the brittleness of the failure mode, and effectively mitigate the shear size effect. The nominal shear strength decreases obviously with an increase in cross-sectional size but increases significantly with an increase in strain rate, exhibiting a pronounced strain rate hardening characteristic. Large-scale beams are more sensitive to strain rate, and a high strain rate can reduce the disparity in shear performance among members of different sizes and further weaken the size effect. Based on Bažant's Size Effect Law (SEL), a modified formula for dynamic shear strength considering the coupled effects of prestress level, strain rate and cross-sectional size was proposed by introducing a prestress enhancement coefficient γ and a strain rate enhancement coefficient β. The calculated results of this formula are in good agreement with the numerical results obtained in this study. Within the investigated parameter range, the present work can provide a reference for the shear design and safety assessment of prestressed recycled aggregate concrete beams under dynamic loading.

Keywords: prestressed RAC beam; prestress level; strain rate; meso-scale numerical simulation; size effect characterization

Check for updates

Academic Editor: Giuseppina Uva

Received: 30 April 2026
Revised: 21 June 2026
Accepted: 23 June 2026
Published: 29 June 2026

Copyright: © 2026 by the authors. Licensee MDPI, Basel, Switzerland. This article is an open access article distributed under the terms and conditions of the Creative Commons Attribution (CC BY) license.

1. Introduction

Recycled Aggregate Concrete (RAC) is a green building material produced by crushing and screening waste concrete to replace natural aggregate. It can effectively utilize construction solid waste and relieve the over-exploitation pressure of natural sand and gravel resources [1,2]. However, recycled coarse aggregate particles are attached with old mortar, have high internal porosity, and feature dual Interfacial Transition Zones (ITZs). As a result, the meso-structure of RAC is more complex than that of natural aggregate concrete,

and its mechanical properties tend to decline with an increase in aggregate replacement ratio, accompanied by significantly increased discreteness [3–6]. Wang et al. [7] found that the splitting tensile strength and elastic modulus decrease with an increase in replacement ratio. Kristensen et al. [8] confirmed through large-scale tests that recycled coarse aggregate with optimized mix proportions can still replace natural aggregate. These studies indicate that heterogeneous material properties are the essential cause of mechanical degradation in RAC.

At the member level, great progress has been made in the shear behavior of reinforced RAC beams. Du et al. [9] conducted shear tests on RAC beams with different replacement ratios (0%, 50%, 100%) and shear span-to-depth ratios. The results show that their failure modes are similar to those of normal concrete beams, but the shear capacity decreases with increasing replacement ratio. Fathifazl et al. [10] obtained similar conclusions for RAC beams with web reinforcement. Notably, Zhao et al. [11] first clearly revealed the size effect phenomenon in shear failure of RAC beams through a series of tests on beams without web reinforcement with different sizes: the nominal shear strength decreases significantly with an increase in section height. Xiao et al. [12] conducted experimental studies on the shear performance of recycled concrete beams and found that their failure modes were similar to those of conventional concrete beams, while their shear capacity decreased with an increase in the replacement ratio of recycled coarse aggregate. However, these experimental studies have a key limitation: they were all conducted under quasi-static loading conditions. The size effect on the shear mechanical behavior of RAC beams under dynamic loading, especially in the presence of prestress, has not yet been addressed. The size effect is an inherent property of quasi-brittle materials such as concrete. Based on nonlinear fracture mechanics, Bažant [13] proposed the classical Size Effect Law (SEL). Bažant et al. [14–16] further extended it to shear failure of reinforced concrete beams and established a theoretical framework for the size effect of shear strength in beams without web reinforcement. Syroka-Korol et al. [17] verified the theory using digital image correlation (DIC). Jin et al. [18,19] found through meso-scale simulations that the stirrup ratio, shear span-to-depth ratio and longitudinal reinforcement ratio all affect the size effect of shear strength. Liu et al. [20] studied the shear behavior and size effect of beams without web reinforcement and found that the nominal shear strength decreases gradually with increasing shear span-to-depth ratio and replacement ratio. In the field of dynamic loading, Park and Krauthammer [21] established a linear elastic fracture mechanics (LEFM)-based dynamic crack criterion for concrete beams and demonstrated that the size effect and rate effect under dynamic loading are not independent phenomena, with the kinetic energy rate being the primary cause of the rate effect. However, the above studies did not consider the rate effect of prestressed RAC beams under dynamic loading. Most of these studies focused on normal concrete or static loading conditions, and the size effect of RAC beams under dynamic loading conditions remains insufficiently studied. Prestressing technology is an effective method to improve the crack resistance and shear performance of concrete members. By introducing a precompressive stress field in the member, tensile stress can be effectively counteracted, the initiation of diagonal cracks can be delayed, and the shear capacity can be improved. Jia et al. [22] confirmed that increasing the prestress level can significantly improve the cracking load and shear capacity. Brandes and Kurama [23] conducted shear tests on prestressed recycled concrete beams with different prestress levels and confirmed that prestressed recycled concrete beams can achieve reliable shear performance under ultimate loading. Jafari et al. [24] performed a systematic numerical study on post-tensioned coupling beams, with the main findings including: a higher initial prestress ratio can reduce damage severity, the axial compression ratio has the greatest influence on damage severity, and increasing the prestress level can delay crack propagation,

reduce damage concentration, and enhance energy dissipation capacity. However, the above studies were either based on conventional concrete or limited to quasi-static/cyclic loading conditions. Abdul-Rahman et al. [25] experimentally investigated the static and dynamic behavior of prestressed concrete under shear loading and confirmed the rate sensitivity of prestressed members, but their work focused on conventional concrete rather than RAC. The combined application of prestressing technology and recycled aggregate concrete under dynamic loading has not yet been systematically investigated, and the influence of prestress level on the shear failure mode and load-carrying capacity of RAC beams under different strain rates remains to be fully clarified.

In practical engineering, concrete structures are often subjected to dynamic loads, such as earthquakes and impacts, and concrete exhibits significant strain rate sensitivity. Fan et al. [26] conducted a comprehensive review and systematic analysis of 116 studies on dynamic increase factor (DIF) and established a mathematical model correlating specimen size and static strength with dynamic strength. They pointed out that static strength has the most significant influence on DIF, followed by specimen size. Jin et al. [27] studied the size effect behavior of concrete under uniaxial compression at different strain rates (10^{-5}/s$\sim$200/s) using meso-scale simulations and found a critical strain rate around 1 s: below this value, the size effect weakens with increasing strain rate; above this value, it strengthens. Jin et al. [28] further found that increasing the strain rate reduces the influence of the confining stress ratio on the biaxial strength size effect. Işık et al. [29] investigated the effects of strain rate (10^{-7}/s$\sim10^{-3}$/s) and specimen size on the direct shear behavior of concrete through push-off tests. The results show that shear strength exhibits a significant rate effect, and its size dependence follows the Type-I Size Effect Law. At the member level, Jin et al. [30], based on the ABAQUS finite element numerical simulation platform, established a three-dimensional meso-scale numerical analysis model, considering the heterogeneity of concrete materials as well as the strain rate effects of both steel reinforcement and concrete. It is found that the nominal shear strength decreases with increasing beam height, while increasing the strain rate and stirrup ratio can enhance the nominal shear strength and mitigate its size effect. Li et al. [31] found that dynamic material properties improve with increasing strain rate, and RAC shows more significant strain rate sensitivity than normal concrete. Nevertheless, none of the above dynamic loading studies involve prestressed RAC beams. In terms of numerical simulation, meso-scale modeling has become an effective tool to reveal the mechanical mechanism of concrete. Naderi and Zhang [32] established a computational framework considering realistic aggregate shapes and found that although irregular aggregate shapes affect microcrack nucleation and fracture patterns, tensile strength is mainly governed by strain rate and aggregate distribution rather than aggregate shape. Liu et al. [33] studied the size effect of RAC under dynamic compression and also obtained a critical strain rate of 1/s. Zhuo et al. [34] verified that Bažant's Size Effect Law is applicable to the compressive behavior of RAC. Nevertheless, the above dynamic studies did not involve prestressed RAC beams, and the synergistic coupling effect of prestress and strain-rate effects on the shear size effect remains completely unexplored.

Based on the above analysis, the following unresolved key issues remain in existing studies: (1) the mechanism by which prestress affects the shear behavior of RAC beams remains unclear, particularly the coupled effects of prestress level, cross-sectional size, and loading rate; (2) the evolution of the size effect in prestressed RAC beams under dynamic loading conditions remains unexplored, and the synergistic mechanism between the precompressive stress field and dynamic loading has not been revealed; and (3) theoretical models for the size effect on shear strength that comprehensively consider the multifactor coupling of prestress level, strain rate, and cross-sectional size are lacking, and

existing modified formulas have not simultaneously introduced prestress and strain-rate enhancement effects.

To fill the above research gaps, a three-dimensional five-phase mesoscopic numerical model is established in this study for the specified parameter conditions. Using this model, the combined influences of prestress level, strain rate and cross-sectional dimension on the dynamic shear performance and size effect of prestressed RAC beams are systematically analyzed. A modified size effect formula is further developed by introducing the prestress enhancement coefficient γ and strain-rate enhancement coefficient β. The research outcomes can serve as a reference for the shear design and safety assessment of prestressed RAC members under dynamic loading within the studied parameter range.

2. Meso-Scale Numerical Analysis Model

2.1. Geometric Model Establishment

Concrete and RAC are typical Heterogeneous Composite Materials. Recycled coarse aggregate particles feature high porosity and abundant microcracks, leading to more significant microstructural variability in RAC than in normal concrete. According to Ref. [35], at the meso-scale, recycled coarse aggregate particles are modeled as spherical particles composed of Five-Phase Composite Material: natural aggregate, Old Interfacial Transition Zone (Old ITZ), old hardened mortar, New Interfacial Transition Zone (New ITZ), and new hardened mortar, as shown in Figure 1. A meso-scale model of recycled coarse aggregate was established using the ABAQUS2020 software, and a 3D random distribution model was generated via a Python 3.12 script to simulate the spatial distribution of aggregates in beams, so as to reproduce the experimental details as accurately as possible. Recycled aggregate follows a two-stage gradation with particle sizes ranging from 20 mm to 40 mm. The number of aggregates is determined by the Fuller Grading Curve [36], expressed as:

$$P = 100\sqrt{\left(\frac{D_0}{D_{\max}}\right)} \tag{1}$$

where P is the mass percentage of aggregates passing the sieve size D_0; D_0 is the sieve diameter; D_{max} is the maximum aggregate size.

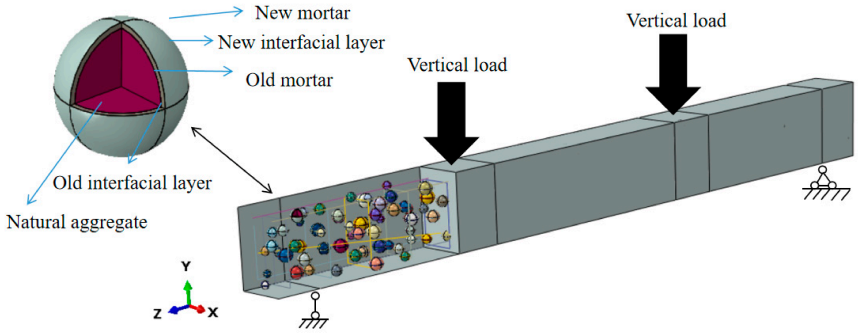

Figure 1. Internal configuration of the RAC beam and mesoscale aggregate model.

For the recycled coarse aggregate phase in prestressed RAC beams, C3D8R solid elements were used. Steel bars and prestressed strands were modeled with T3D2 truss elements. Two rigid loading blocks were set at the loading points, and their midlines were coupled to a reference point P. Displacement-controlled loading was applied to point P so that the loading blocks could rotate with the bending deformation of the beam, avoiding artificial stress concentration and damage to the beam caused by constrained rotation of the loading blocks. One support was fixed with displacement constraints in X, Y, and Z directions and rotational constraints around Y and Z axes. The other support was

constrained in X and Y directions and restrained against rotation around Y and Z axes to simulate simply supported boundary conditions.

Regarding the correctness of the spherical modelling of recycled concrete coarse aggregates, the following two aspects are mainly considered: (1) The effect of the spherical assumption on crack propagation. Quantitative assessments of the difference between spherical and realistic aggregate shapes are available in the literature. Naderi and Zhang [32] compared spherical and realistic aggregate shapes in meso-scale simulations of concrete tensile fracture. They found that the aggregate shape affects the nucleation site and local propagation pattern of microcracks but has no significant effect on the macroscopic tensile strength; the tensile strength depends mainly on the strain rate and the spatial distribution of aggregates. (2) Effect of the spherical assumption on shear response. Under shear loading, the angularities of irregular aggregates may enhance the mechanical interlock at the aggregate–mortar interface, whereas spherical aggregates have smooth surfaces and may thus underestimate the aggregate interlock and friction energy dissipation along the crack surface. However, existing studies [37–40] indicate that the strength characteristics of the ITZ, the aggregate volume fraction, and the spatial distribution of aggregates are more dominant factors governing the macroscopic shear strength of members.

2.2. Bond–Slip Relationship and Prestress Application

In actual beams, steel reinforcement and recycled aggregate concrete (RAC) exhibit cooperative deformation and bond stress. To reflect the interaction between bottom longitudinal reinforcement, prestressing strands and RAC in the model, the bond–slip relationship for reinforced concrete recommended by Code [41] is adopted. The bottom longitudinal reinforcement, prestressing strand and other reinforcement are connected to RAC by nonlinear spring elements. By considering the bond–slip behavior between reinforcement and concrete in the ABAQUS modeling of reinforced concrete beams, the actual interaction behavior between the two materials can be better reproduced, so that the obtained load–displacement curve, crack propagation, reinforcement stress variation and final failure mode are closer to the test results.

The prestress was applied to the prestressing strand using the cooling method. This method achieves equivalent prestressing through thermal expansion and contraction, and the temperature load is applied uniformly and controllably, resulting in a more uniform stress distribution in the strands. It can better restore the actual prestressing process, form a stable precompressive stress inside the concrete, and further improve the calculation accuracy of the finite element model. Specifically, a controllable temperature field was applied to the prestressing strands, and the temperature was gradually reduced from normal temperature to $-440\ ^{\circ}\mathrm{C}$ to induce contraction deformation of the strands. Tensile stress is thus established in the prestressing strands, and equivalent precompressive stress is formed in the concrete, which is equivalent to the mechanical state achieved by the traditional tensioning process and meets the prestress level requirements of the model test. The same prestress value as in the test was calculated by Equation (2), thereby producing the same prestress effect as the test. The reinforcement layout of the prestressing strand is shown in Figure 2.

$$\Delta T = \frac{\sigma}{E \cdot \alpha} \tag{2}$$

where: ΔT is the temperature reduction; σ is the stress; α is the coefficient of thermal expansion; E is the elastic modulus.

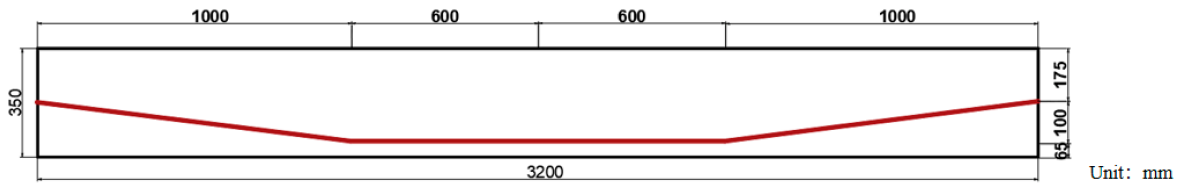

Figure 2. Schematic layout of prestressing reinforcement in prestressed recycled aggregate concrete (RAC) beam.

When the thermal cooling method is used to apply prestress, its basic assumptions are as follows. (1) Uniform temperature field: a uniform temperature reduction is applied along the full length of the strand, which can make the stress distribution along the strand more uniform. (2) Elastic thermal contraction: the strain of the strand depends only on Equation (2). In the present simulation, −440 °C is only the numerical temperature difference used to reproduce the prestress in the strand, rather than the actual physical temperature of the strand. In the finite element analysis, it serves only as a control parameter for generating the target contraction strain and does not involve material properties at low temperature. (3) No prestress loss: time-dependent losses caused by concrete shrinkage and creep, strand relaxation, and anchorage deformation are not considered. The model reflects an ideal state immediately after prestress application.

This study aims to investigate the coupled effects of prestress level, strain rate, and cross-sectional size on the dynamic shear performance of RAC beams. It is a parametric mechanistic study, with the main focus on the crack-suppression behavior induced by different initial effective prestress levels rather than on the long-term time-dependent behavior of the prestressing system. Regarding prestress loss, shrinkage, creep, and relaxation are all long-term effects, while the short-term dynamic loading process simulated in this study is much shorter than their time scales; therefore, neglecting long-term losses does not affect the comparative conclusions. Regarding transfer length, the critical diagonal crack is located in the middle of the flexural-shear span, beyond the typical transfer length range from the beam end, namely 50–80 times the strand diameter. Thus, a uniform prestress field provides an equivalent approximation of the stress state in this region.

Limitations: this method cannot capture bond stress concentration and end microcracks within the transfer length region, cannot simulate long-term prestress loss, and cannot characterize the detailed stress state in the anchorage zone. For studies involving the above issues, more refined modeling strategies are required. In summary, the thermal cooling method is applicable and computationally efficient within the framework of this study, and its simplifications do not affect the validity of the main conclusions.

2.3. Constitutive Relationships

The constitutive model of steel reinforcement adopts a bilinear elastic-hardening model. The yield strength is determined by measured values from material property tests, the elastic modulus is selected according to conventional values, and Poisson's ratio is set to 0.3. The constitutive model of prestressing strands adopts the no-yield point reinforcement model built into ABAQUS2020. The concrete damage plasticity model embedded in the software is used to define relevant damage and plasticity parameters. The mechanical performance parameters of five-phase materials, including natural aggregate, old mortar, new mortar, old interfacial transition zone and new interfacial transition zone, are determined by the constitutive curves proposed in the literature [42]. The specific values are listed in Table 1.

Table 1. Material property parameters.

Parameter Category	Natural Aggregate	Old Mortar	New Mortar	Old ITZ	New ITZ
Elastic modulus (GPa)	80.00	19.27	23.68	19.27	23.68
Poisson's ratio	0.16	0.22	0.22	0.20	0.20
Compressive strength (MPa)	80.00	18.17	26.78	10.20	12.20
Compressive strain	——	3.77×10^{-3}	2.80×10^{-3}	3.77×10^{-3}	2.80×10^{-3}
Ultimate strength (MPa)	——	6.06	8.93	3.40	4.06
Ultimate strain	——	0.010	0.008	0.010	0.008
Tensile strength (MPa)	10.00	1.66	1.91	1.02	1.22
Tensile strain	——	1.0×10^{-4}	1.0×10^{-4}	1.0×10^{-4}	1.0×10^{-4}
Dilation angle (°)	——	38	38	35	35
Eccentricity e	——	0.1	0.1	0.1	0.1
Viscosity parameter μ	——	1.0×10^{-4}	1.0×10^{-4}	5.0×10^{-5}	5.0×10^{-5}
Tensile fracture energy Gf (N/m)	——	80	95	30	38
Compressive fracture energy Gc (N/m)	——	8000	9500	3000	3800

2.3.1. Damage Evolution and Fracture Energy Regularization

The CDP model defines the compressive damage dc and the tensile damage d_t as functions of the corresponding inelastic/cracking strains. In this paper, the compressive damage evolution follows a linear relationship:

$$d_c = 1 - \frac{\sigma_c}{f_c} \text{ when } \sigma_c > f_c \tag{3}$$

Here, σ_c is the compressive stress; f_c is the axial compressive strength of concrete. The tensile damage evolution follows an exponential softening law:

$$d_t = 1 - \exp\left(-\frac{\varepsilon_t^{ck}}{\varepsilon_{t,ref}^{ck}}\right) \tag{4}$$

Here, ε_t^{ck} is the cracking strain; $\varepsilon_{t,ref}^{ck}$ is the reference cracking strain.

To get rid of the common mesh sensitivity issue in the finite-element simulation of quasi-brittle materials and ensure the objectivity of energy dissipation (independent of element size), this paper uses the crack band model originally proposed by Bažant and Oh [43]. This method links the fracture energy G_f to the post-peak stress-displacement response instead of the stress–strain response. The ultimate tensile cracking displacement u_{ck} is expressed as:

$$u_{ck} = \frac{2G_f}{f_t} \tag{5}$$

Here, f_t is the axial tensile strength of concrete. The cracking strain ε_t^{ck} is related to the cracking displacement u_{ck} through the characteristic element length l_{ch}:

$$l_{ch} = \sqrt[3]{V_e} \tag{6}$$

(for 3D solid elements), where V_e is the volume of the finite element. So, the reference cracking strain $\varepsilon_{t,ref}^{ck}$ is determined as:

$$\varepsilon_{t,ref}^{ck} = \frac{u_{ck}}{l_{ch}} = \frac{2G_f}{f_t \cdot l_{ch}} \tag{7}$$

Similarly, the inelastic strain at compression failure is regularized as follows:

$$\varepsilon_{c,u}^{in} = \frac{2G_c}{f_c \cdot l_{ch}} - \frac{f_c}{E_0} \tag{8}$$

where E_0 is the initial elastic modulus of the material.

2.3.2. Rate-Dependent Constitutive Models

Both concrete and reinforcing steel are strain-rate-sensitive materials. To account for the material strain-rate effect in dynamic simulations, the following rate-dependent constitutive models are adopted. The dynamic compressive strength, dynamic tensile strength, and dynamic elastic modulus of concrete are enhanced using the dynamic increase factor formulas recommended by fib Model Code 2010:

Compressive dynamic increase factor (CDIF):

$$\frac{f_{cd}}{f_c} = \begin{cases} \left(\dot{\varepsilon}_c/\dot{\varepsilon}_{cd}\right)^{0.014}, \ \dot{\varepsilon}_c \le 30\ s^{-1} \\ 0.012\left(\dot{\varepsilon}_c/\dot{\varepsilon}_{cd}\right)^{1/3}, \ \dot{\varepsilon}_c > 30\ s^{-1} \end{cases} \tag{9}$$

Tensile dynamic increase factor (TDIF):

$$\frac{f_{td}}{f_t} = \begin{cases} \left(\dot{\varepsilon}_t/\dot{\varepsilon}_{td}\right)^{0.018}, \ \dot{\varepsilon}_t \le 10\ s^{-1} \\ 0.0062\left(\dot{\varepsilon}_t/\dot{\varepsilon}_{td}\right)^{1/3}, \ \dot{\varepsilon}_t > 10\ s^{-1} \end{cases} \tag{10}$$

Elastic modulus dynamic increase factor (MDIF):

$$\frac{E}{E_0} = \left(\frac{\dot{\varepsilon}_c}{\dot{\varepsilon}_0}\right)^{0.026} \tag{11}$$

The quasi-static strain rates are taken as $\dot{\varepsilon}_{cd} = 3.0 \times 10^{-5}\ s^{-1}$, $\dot{\varepsilon}_{td} = 1.0 \times 10^{-5}\ s^{-1}$, $\dot{\varepsilon}_0 = 3.0 \times 10^{-5}\ s^{-1}$. These formulas are applied to update the mechanical parameters of the mortar matrix, the interfacial transition zone (ITZ), and the aggregates (treated as strengthened mortar), thereby explicitly introducing material strain-rate sensitivity at the meso-scale.

Regarding the strain-rate effect of reinforcing steel, the dynamic yield strength and dynamic ultimate strength also increase with strain rate:

$$\frac{f_{yd}}{f_0} = 1.0 + \left(\frac{6}{f_0}\right) \ln \frac{\dot{\varepsilon}}{\dot{\varepsilon}_0}, \ \frac{f_{ud}}{f_0} = 1.0 + \left(\frac{7}{f_0}\right) \ln \frac{\dot{\varepsilon}}{\dot{\varepsilon}_0} \tag{12}$$

The quasi-static strain rate is taken as $\dot{\varepsilon}_0 = 5.0 \times 10^{-4}\ s^{-1}$.

2.4. Dynamic Loading and Strain Rate Handling

Concrete shows significant strain rate sensitivity under dynamic loads, and its strength is usually characterized by the dynamic increase factor (DIF, which is the ratio of dynamic strength to static strength). The dynamic shear failure of prestressed RAC beams involves multiple rate-related mechanisms at the material and structural levels. To ensure the reproducibility of numerical results and give a physically reasonable explanation for the observed strain rate sensitivity, this section systematically explains the numerical solution strategy, loading regime, handling method of inertial effects, and damping assumptions.

2.4.1. Solution Scheme and Time Integration

All the dynamic simulations were conducted using the ABAQUS/Explicit solver, which employs the central difference time integration scheme. This choice was based on the highly nonlinear characteristics of this problem—involving concrete cracking, bond–slip

degradation, and multi-axial stress states—under medium to higher loading rates (10^{-3}/s to 10/s). The explicit central difference operator satisfies the dynamic equilibrium equation at time t:

$$M\ddot{u}|_t + F^{int}|_t = F^{ext}|_t \quad (13)$$

Wherein M is the consistent mass matrix, $\ddot{u}$ is the vector of nodal accelerations, F^{int} is the internal force vector derived from the element stress, and F^{ext} is the external load vector. The nodal accelerations are directly calculated from the mass matrix without the need for iteration, making the explicit method particularly suitable for high-speed dynamic problems with material degradation. The stable time increment Δt in the explicit scheme is automatically determined by the element-wise Courant–Friedrichs–Lewy (CFL) condition:

$$\Delta t = \min\left(\frac{L_e}{c_d}\right) \quad (14)$$

Wherein Le is the element characteristic length, and c_d is the expansion wave velocity of the material, given by the following formula:

$$c_d = \sqrt{\frac{E(1-\nu)}{(1+\nu)(1-2\nu)\rho}} \quad (15)$$

where E, ν and ρ are the material's elastic modulus, Poisson's ratio, and density, respectively. For the 30 mm grid size used in this study, the stable time increment is approximately between 4.2×10^{-7} s and 6.8×10^{-7} s, depending on the local material stiffness. No mass scaling was used in the simulation, and the default enhanced stiffness hourglass control was employed to suppress false zero-energy modes. The total increment steps required for a single dynamic analysis vary from approximately 1.5×10^5 steps at the lowest strain rate (10^{-5}/s) to approximately 1.5×10^7 steps at the highest strain rate (10/s). All the simulations were completed on a high-performance computing cluster equipped with 48-core CPUs.

2.4.2. Loading Scheme and Displacement–Strain Rate Relationship

The simulation adopts a displacement-controlled loading scheme. The vertical displacement is applied at the reference point P coupled with the loading block at the top, allowing the loading block to rotate along with the bending deformation of the beam to avoid artificial stress concentration at the loading point.

To minimize false dynamic oscillations, the displacement loading uses a smooth step amplitude function (smooth step amplitude curve), ensuring zero initial velocity and zero initial acceleration at the initial loading time, and then smoothly transitions to the target velocity. Ensure zero initial velocity and zero initial acceleration, and the loading history includes an ascending segment of 0.01 s and a subsequent constant speed segment. The nominal strain rate is $\dot{\varepsilon} = v/h_0$ (11), where v is the displacement rate in the constant speed segment and h_0 is the effective height of the beam cross-section.

2.4.3. Handling of Inertial Effects and Distinction from Material Rate Sensitivity

One of the key issues in numerical simulation of the dynamic behavior of concrete is how to distinguish the structural inertial effects from the actual material strain rate sensitivity. This distinction has been widely discussed in the field of concrete dynamics. Zhou and Hao [37] used homogeneous macroscopic models and heterogeneous microscopic models to conduct numerical analysis of the compressive behavior of concrete-like materials at high strain rates. They first assumed that the material properties were independent of the rate, and the results showed that only inertial constraints could produce apparent dynamic

strength enhancement; subsequently, they introduced rate-sensitive material properties and investigated the relative contributions of inertial effects and material rate effects to the compressive DIF. The research results indicated that when the strain rate was approximately lower than 100/s, the dynamic strength enhancement was mainly attributed to the material rate sensitivity of the mortar matrix; while at higher strain rates, the influence of inertial constraints gradually became significant. According to the investigations reported in Refs. [44–47], different strain-rate ranges correspond to different loading types. Generally, when the strain rate is within 10^{-8}~10^{-6} s^{-1}, the loading condition can be regarded as a creep state, corresponding to sustained loading. When the strain rate ranges from 10^{-5}~1 s^{-1}, it can be considered as quasi-static to intermediate strain-rate loading, corresponding primarily to seismic loading. When the strain rate ranges from 10^{1}~10^{3} s^{-1}, it is regarded as a high-strain-rate loading condition, corresponding to impact and blast loading. In this study, the variation law of the shear capacity of beams was analyzed within the prescribed strain-rate range of 10^{-5}~10 s^{-1}. Within the strain-rate range of 10^{-5}~1 s^{-1}, the increase in shear capacity is mainly attributed to the strain-rate sensitivity of the material. When the strain rate ranges from 1~10^{1} s^{-1}, corresponding to low-velocity impact loading, the enhancement in shear capacity results from the combined effects of material strain-rate sensitivity and structural inertia effects. The strain-rate range investigated in this study (10^{-5}~10 s^{-1}) covers the quasi-static to intermediate strain-rate regime and partially enters the transitional regime. The observed increase in shear capacity with loading rate in this study originates from two sources: (1) the material strain-rate sensitivity explicitly captured by the DIF formulas, and (2) the structural inertial effects automatically accounted for by the explicit dynamic solver (ABAQUS/Explicit) through the mass acceleration term (Equation (13)). It should be emphasized that the current mesoscopic finite element model fails to distinguish the respective influences of material sensitivity and structural inertia on experimental results. Therefore, the term "strain rate effect" adopted in this paper refers to the combined dynamic response induced jointly by the two factors above.

2.4.4. Damping Assumptions

No additional global damping was introduced into the numerical model. This conservative assumption avoids artificial suppression of high-frequency dynamic response, which may affect crack propagation patterns and energy dissipation characteristics under high strain rate. The low-level numerical damping inherent to the central difference time integration scheme of ABAQUS/Explicit is introduced via bulk viscosity parameters and retained at default values: linear bulk viscosity parameter b_1 = 0.06 and quadratic bulk viscosity parameter b_2 = 1.2. These parameters moderately suppress high-frequency numerical noise, with negligible physical damping introduced.

2.5. Model Validation

Based on the aforementioned meso-scale modeling approach, the specimens CRCB-1 and CRCB-2 with a cross-sectional size of 200 mm × 350 mm from Ref. [48] were selected for shear failure simulation. The specimen had a recycled aggregate replacement ratio of 0, a shear span-to-depth ratio of 2.66, a reinforcement ratio of 1.03%, a stirrup ratio of 0.141%, and a designed concrete strength of 40.69 MPa. In the prestressed recycled aggregate concrete beams used for testing, three different grades of reinforcement were used: 20 mm HRB400 deformed bars as longitudinal reinforcement, 12 mm HRB400 deformed bars as erection reinforcement, and 6 mm HPB300 plain bars as stirrups. The mechanical properties of the reinforcement are listed in Table 2. The prestressing strands had a yield strength of

1860 N/mm^2, an ultimate strength of 1923 N/mm^2, an elongation of 5.5%, and an elastic modulus of 1.94 × 10^5 N/mm^2.

Table 2. Types and mechanical properties of reinforcement in specimens CRCB-1 and CRCB-2 (Ref. [48]).

Reinforcement Type	Diameter/mm	Elastic Modulus/GPa	Yield Strength/MPa	Ultimate Strength/MPa
HRB300	6	228	318	529
HRB400	12	217	436	574
	20	215	428	570

The comparison between the experimental and simulated failure modes of prestressed recycled concrete beams is shown in Figure 3. The variation in plastic strain w from 0 to 0.003 corresponds to the transition of the specimen from the intact state to the failure state. As shown in Figure 3, the simulated results for specimens CRCB-1 and CRCB-2 at the beam side and beam bottom are basically consistent with the experimental results, and the damage state of the model is in good agreement with the actual failure state of the beams in the tests. Therefore, the model can be used for subsequent simulations. To clarify the influence of different mesh parameters on the simulation results, three different element mesh densities, 1 cm, 2 cm, and 3 cm, were established, and the corresponding load–displacement curves are shown in Figure 4. For specimens CRCB-1 and CRCB-2, the load–displacement curves obtained with the three mesh sizes are basically consistent with the experimental ones. As shown in Figure 4, the simulation accuracy improves as the mesh density increases, and the maximum error occurs when the mesh size is 3 cm. When the mesh size is 3 cm, the simulated loads of specimens CRCB-1 and CRCB-2 are 178.54 kN and 258.55 kN, respectively, while the experimental loads are 165.13 kN and 240.50 kN, respectively. The maximum error is 8.12%, which is less than 10% and meets the accuracy requirements for subsequent studies. Based on the Fuller grading curve described in Section 2.1, i.e., Equation (1), and the two-stage particle size distribution of 20–40 mm, three aggregate spatial random placement schemes denoted as R1, R2, and R3 were regenerated using a Python 3.12 script combined with the Monte Carlo method, with the original model denoted as R0. In each scheme, the total aggregate volume fraction, particle size range, and gradation were kept constant, and only the spatial positions and local adjacency relationships of aggregate particles were varied. Specimen CRCB-2 from Ref. [48] was simulated, and the results show that the four models exhibited consistent failure modes. The shear capacities were 258.550 kN, 259.667 kN, 259.157 kN, and 257.715 kN, respectively, with a maximum difference of less than 0.5%, which meets the accuracy requirements. Based on the above comparative analysis, the meso-scale model agrees well with the actual experimental behavior and can be used for subsequent studies. Considering both computational efficiency and computational accuracy, a mesh size of 3 cm was adopted for all models. The present model was validated against two quasi-static prestressed recycled concrete beam specimens reported in Ref. [48], including comparisons of failure modes and load–displacement curves. The subsequent analyses in this study involve extended conditions with multiple sectional sizes, different prestress levels, and a wide range of dynamic strain rates, for which no publicly available third-party experimental data are currently available for corresponding validation. Combined with the results of mesh convergence analysis and sensitivity analysis of random aggregate distribution, the model can be demonstrated to possess satisfactory computational stability under the unified modeling framework adopted in this study. However, the simulation accuracy under dynamic loading conditions still requires further validation through future experimental investigations.

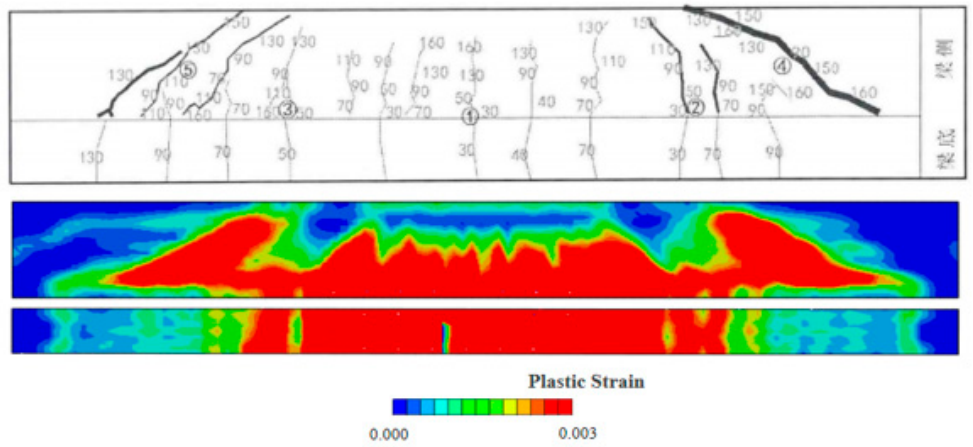

(**1**)

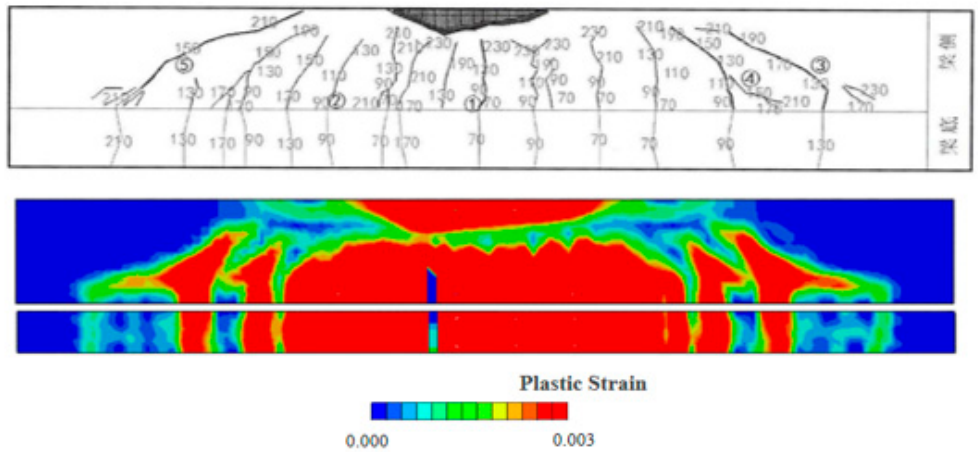

(**2**)

Figure 3. Comparison of beam failure modes between experiment and simulation. (**1**) Comparison between experimental test and simulated failure patterns of specimen CRCB1 in Ref. [48]; (**2**) Comparison of experimental and simulated failure modes for specimen CRCB2 from Reference [48].

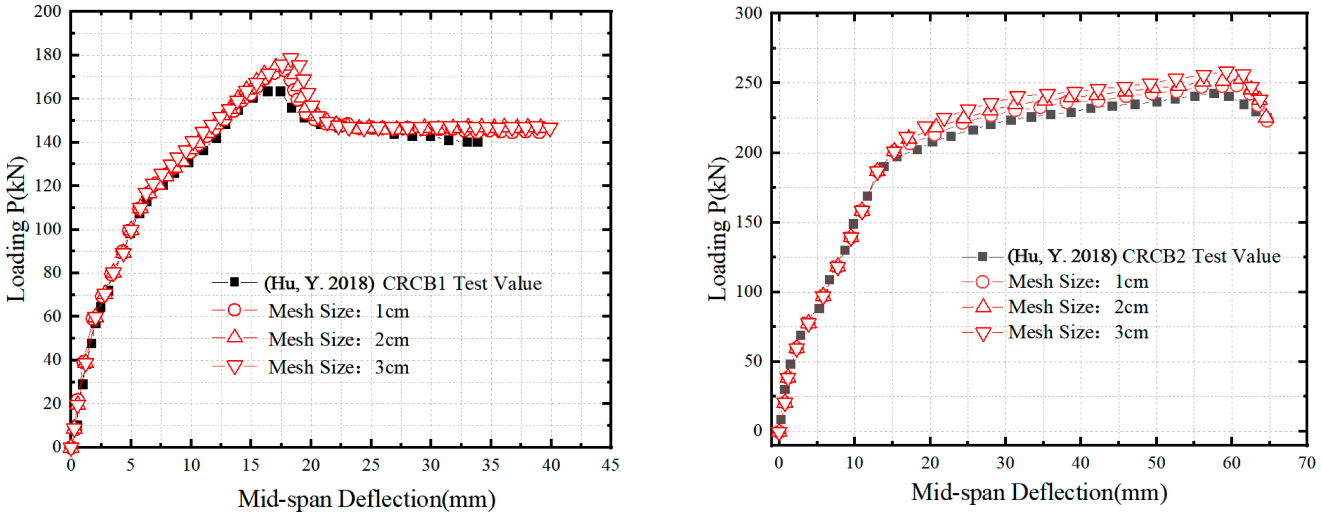

Figure 4. Comparison of load–displacement curves between the experiment and the numerical model in this paper [48].

3. Shear Performance and Size Effect of Prestressed RAC Beams Under Different Prestress Levels

3.1. Failure Modes Under Different Prestress Levels

By varying the prestress level, the shear failure modes and size effects of beams at a dynamic loading strain rate of 10^{-5}/s were investigated. The reinforcement ratio, stirrup ratio, and shear span-to-depth ratio were set to 1.03%, 0.141%, and 2.1, respectively. The prestress levels were 0, 0.228, and 0.431, respectively, with a recycled aggregate replacement ratio of 30%. The cross-sectional dimensions were 200 mm × 350 mm, 300 mm × 525 mm, and 400 mm × 700 mm, resulting in a total of nine prestressed RAC beams. The corresponding geometric parameters of the beams are listed in Table 3. In this paper, the lowest strain rate of 10^{-5}/s corresponds to a displacement rate of 3.15×10^{-3}–6.30×10^{-3} mm/s, which is regarded as the quasi-static condition; the range of 10^{-3}–10^{-1}/s is classified as the low dynamic regime, and 1–10/s as the high dynamic regime.

Table 3. Geometric parameters of prestressed RAC beams under different prestress levels.

Specimen	Cross-Sectional Dimension $b \times h$/mm	Beam Length/mm	Replacement Ratio r%	Shear Span-to-Depth Ratio λ	Prestress Level k	Strain Rate $\dot{\varepsilon}$/s
DRAC-Sa1	200 × 350	3200	30	2.1	0	10^{-5}
DRAC-Sa2	200 × 350	3200	30	2.1	0.228	10^{-5}
DRAC-Sa3	200 × 350	3200	30	2.1	0.431	10^{-5}
DRAC-Ma1	300 × 525	4200	30	2.1	0	10^{-5}
DRAC-Ma2	300 × 525	4200	30	2.1	0.228	10^{-5}
DRAC-Ma3	300 × 525	4200	30	2.1	0.431	10^{-5}
DRAC-La1	400 × 700	6200	30	2.1	0	10^{-5}
DRAC-La2	400 × 700	6200	30	2.1	0.228	10^{-5}
DRAC-La3	400 × 700	6200	30	2.1	0.431	10^{-5}

Under the conditions of a strain rate of 10^{-5}/s, a recycled aggregate replacement ratio of 30%, and a shear span-to-depth ratio of 2.1, the effects of different prestress levels on the shear failure modes and size effects of prestressed RAC beams are illustrated in Figure 5. The comparison of failure patterns indicates that the prestress level significantly affects crack development, failure brittleness, and the evolution of the size effects. When the prestress level is zero, numerous cracks are observed in the beam, with irregular distributions. The diagonal cracks are short and wide and propagate rapidly. Pronounced local crushing occurs in the shear-compression zone, and the overall behavior exhibits typical brittle shear failure. Moreover, as the sectional size increases, cracks become more concentrated and brittleness becomes more evident, indicating a significant size effect. When the prestress level increases to 0.228, the number of cracks decreases markedly; the main diagonal cracks become clearer, more slender, and more uniformly distributed; the crack width decreases; and crack propagation slows down. The crushing region is reduced, and failure brittleness is significantly alleviated. Meanwhile, the differences in failure modes among beams of different sizes are reduced, indicating a substantial weakening of the size effect. When the prestress level further increases to 0.431, the number of cracks is minimized, and the principal diagonal cracks become slender and well-defined, with noticeably delayed crack development.

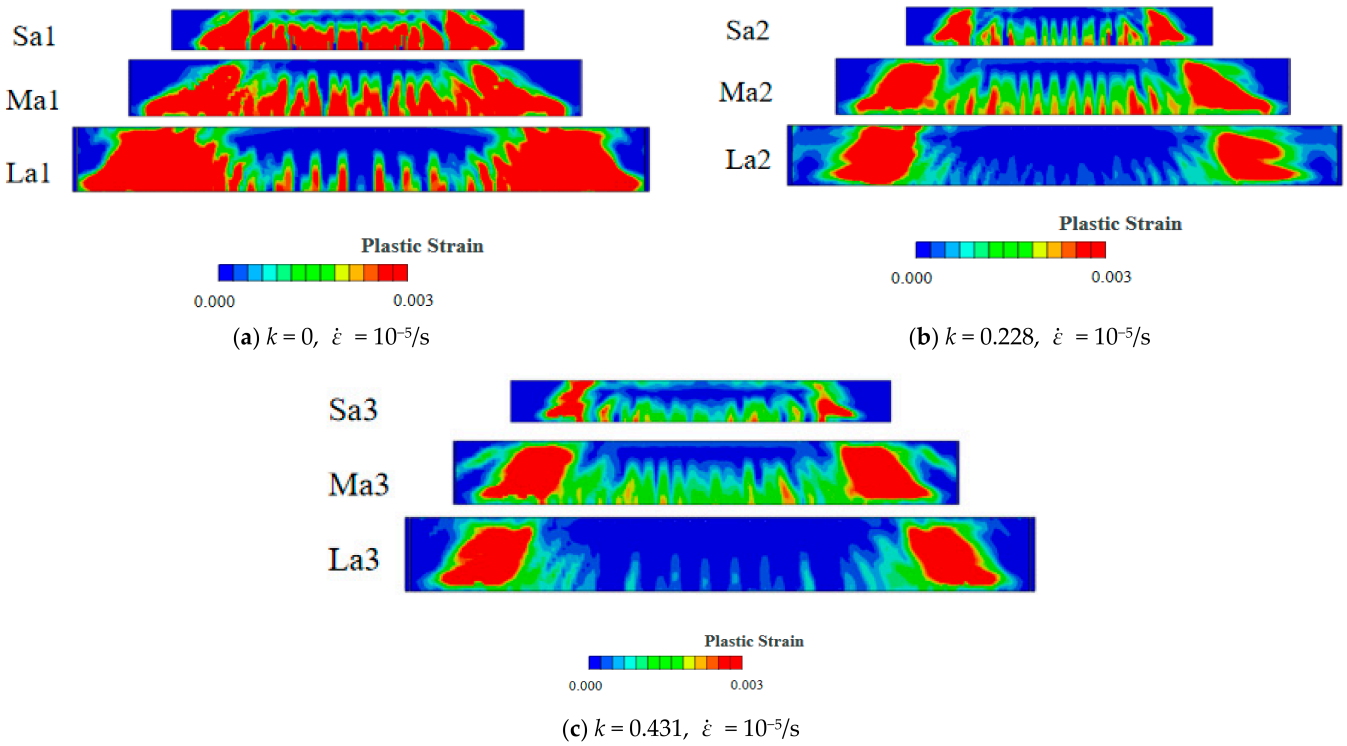

(**a**) $k = 0$, $\dot{\varepsilon} = 10^{-5}$/s (**b**) $k = 0.228$, $\dot{\varepsilon} = 10^{-5}$/s

(**c**) $k = 0.431$, $\dot{\varepsilon} = 10^{-5}$/s

Figure 5. Failure modes of prestressed RAC beams under different prestress levels.

The above phenomena can be analyzed from two aspects: the variation of stress states in cracked zones and the frictional effect at crack interfaces. Prestress generates a persistent compressive stress field inside the beam member, which compensates for the high porosity defect of recycled concrete materials. After acting on the surfaces of inclined cracks, prestress produces a compaction effect that effectively counteracts the tensile stress required for crack initiation and propagation, thereby delaying the emergence and extension of cracks [22]. Meanwhile, the compressive prestress elevates the contact pressure between the two sides of the cracks, further strengthening the interlocking action between aggregates and the interfacial friction effect [24] and rendering the crack development process gentler and more stable. At relatively high prestress levels, the tensile propagation tendency of the cracks is significantly restrained. Combined with the improved energy dissipation capacity of interfacial friction, this mechanism can effectively avoid brittle crushing failure induced by the simultaneous rapid growth of multiple cracks. Accordingly, the failure mode of the component transforms gradually from dispersed brittle failure with numerous microcracks to a ductile failure pattern characterized by the slow propagation of a single primary crack [23]. A higher prestress level corresponds to a more prominent restraining effect on the cracks, a later moment of full crack penetration, and less abrupt component failure. This may serve as the intrinsic mechanism whereby prestress effectively mitigates the aggravation of brittleness caused by the size effect.

3.2. Load–Displacement Curves Under Different Prestress Levels

As shown in Figure 6, under a dynamic loading strain rate of 10^{-5}/s, a recycled aggregate replacement ratio of 30% and a shear span-to-depth ratio of 2.1, dynamic loading simulations were performed on small-sized (200 mm × 350 mm), medium-sized (300 mm × 525 mm), and large-sized (400 mm × 700 mm) prestressed RAC beams. The load–displacement curves and ultimate shear capacities under three prestress levels (0, 0.228, and 0.431) were compared. At a prestress level of 0, the ultimate shear capacities for the small-, medium-, and large-sized beams were 227.07, 495.40, and 766.21 kN, respec-

tively. At a prestress level of 0.228, the corresponding values increased to 260.21, 568.53, and 897.30 kN, respectively, and further increased to 304.16, 682.15, and 1103.91 kN at a prestress level of 0.431. For beams with the same cross-sectional dimension, the ultimate shear capacity increased clearly with increasing prestress level. The higher the prestress level, the greater the enhancement in load-carrying capacity. For small beams, increasing the prestress level from 0 to 0.228 and 0.431 increased the capacity by 14.59% and 33.93%, respectively; for medium beams, the increases are 14.76% and 37.70%, respectively; and for large beams, the increases are 17.11% and 44.07%, respectively. This is because the application of prestress can effectively suppress the initiation and propagation of shear cracks in the beam body, reduce the shear damage of the cross-section, and thus improve the ultimate shear capacity. Moreover, this enhancement effect becomes stronger as the size of the beam body increases. The displacement ductility coefficient $\mu = \Delta u/\Delta y$ was adopted as the quantitative indicator, where Δu is defined as the displacement corresponding to the load dropping to 85% of the peak load value, and Δy is determined by the equivalent energy method. For large-sized beams, the μ value increased from 1.65 at k = 0 to 2.92 at k = 0.431, with an increase rate of 77%. This quantitatively verifies that increasing the prestress level can effectively reduce the brittleness of failure.

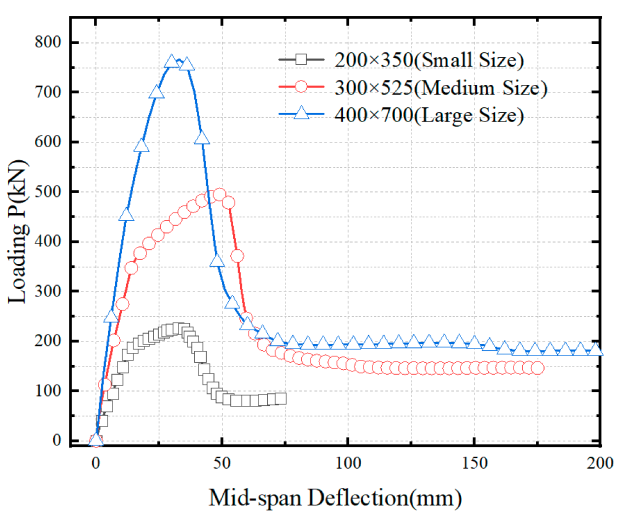

(**a**) $k = 0$

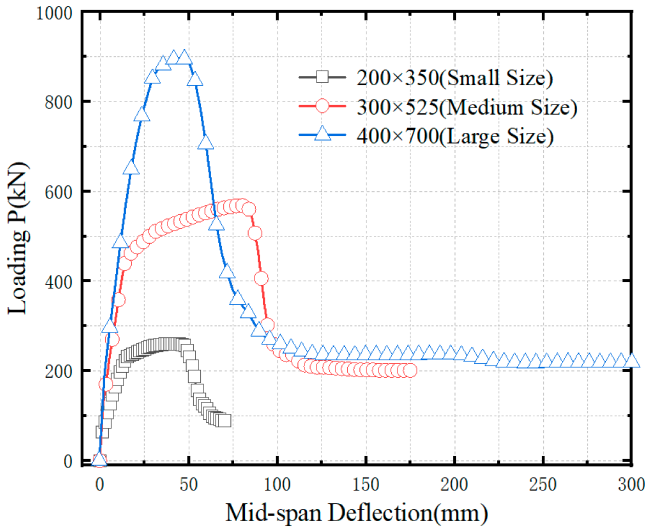

(**b**) $k = 0.228$

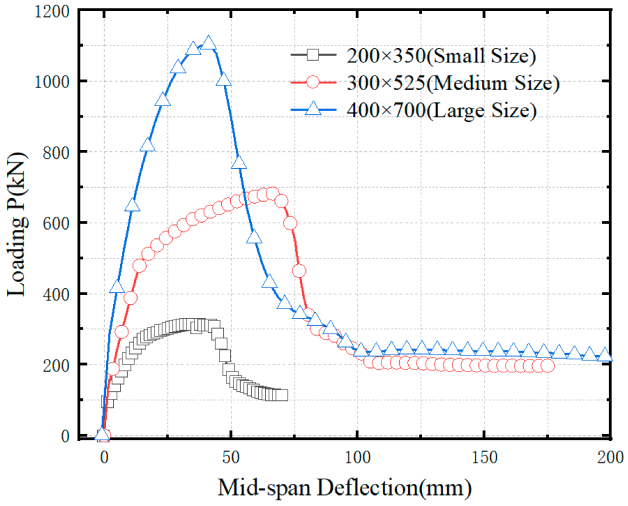

(**c**) $k = 0.431$

Figure 6. Load–displacement curves of prestressed RAC beams under different prestress levels.

Based on the staged analysis method for damage evolution of prestressed members, the shear failure process of prestressed RAC beams can be divided into four stages. Elastic Stage: The external load is small, the principal tensile stress in the flexural-shear region has not yet reached the tensile strength of concrete, the beam body is in an elastic working state, and the load–displacement curve exhibits a linear trend. Crack Initiation Stage: The principal tensile stress in the flexural-shear region reaches the tensile strength of the ITZ or mortar matrix in RAC, and the first batch of microcracks initiates at weak positions such as the ITZ. The precompressive stress field induced by prestress offsets part of the tensile stress and increases the load level required for crack initiation. The higher the prestress level, the later the crack initiation occurs and the greater the cracking load. Stable Crack Propagation Stage: As the load increases, the number of microcracks increases and they gradually coalesce into visible diagonal cracks, with the width and length of the cracks increasing continuously. At this stage, the prestress level exerts a dual effect: first, the precompressive stress at the crack tip reduces the net K_I, restricting the further opening of the crack; second, the normal compressive stress on the crack surface enhances the aggregate interlock friction, enabling the cracked cross-section to still maintain considerable shear transfer capacity. Under a high prestress level, the crack propagation rate is effectively controlled, which is manifested as slender cracks with slow development. Unstable Failure Stage: After the load reaches the peak value, the main diagonal crack rapidly penetrates the cross-section and the member loses its load-bearing capacity. Due to the persistent precompressive stress field in highly prestressed beams, the failure mode transforms from diffuse brittle failure to the controlled propagation of a single dominant crack. The higher the prestress level, the stronger the restraining effect on cracks, the more delayed the crack penetration, and the lower the abruptness of failure.

The test data indicate that prestress improves the bearing capacity of small-sized beams by 33.93%, while the enhancement ratio for large-sized beams reaches 44.07%. It can be seen that the strengthening effect of prestress is more remarkable in large-scale members. The underlying mechanisms are illustrated as follows. On the one hand, increasing the prestress level can retard the interconnection and full penetration of internal microcracks inside members, slowing down the crack propagation rate [22]. On the other hand, the internal compressive stress induced by prestress further strengthens the aggregate interlocking and interfacial friction at crack surfaces, which comprehensively improves the shear-bearing capacity of beams [24]. Large-sized beams are more severely affected by the material deterioration of recycled concrete and inherently possess weaker shear resistance. For this reason, prestress exerts a more significant improvement on their bearing capacity, thereby effectively weakening the size effect on the shear performance of recycled concrete beams [23].

3.3. Effect of Prestress Level on the Nominal Shear Strength of Beams

The relationship between the shear strength of prestressed recycled concrete beams and the sectional dimensions was analyzed using the nominal shear strength τ_u:

$$\tau_u = P_u / (b h_0) \tag{16}$$

where P_u is the peak load, b is the section width of the beam, and h_0 is the effective height of the beam section.

As shown in Figure 7, under the dynamic loading strain rate of 10^{-5}/s, and under the conditions of 30% replacement ratio of recycled aggregates and a shear span-to-depth ratio of 2.1, dynamic loading simulations were conducted on small-sized (200 mm × 350 mm), medium-sized (300 mm × 525 mm), and large-sized (400 mm × 700 mm) prestressed recycled concrete beams. The nominal shear strengths under three prestress levels (0,

0.228, 0.431) were compared. At a prestress level of 0, the nominal shear strengths of the small-, medium-, and large-sized beams were 3.78, 3.476, and 3.064 MPa respectively; at a prestress level of 0.228, the cross-section increased from small size to medium size and then to large size, and the nominal shear strengths were 4.34, 3.98, and 3.76 MPa, respectively; at a prestress level of 0.431, the cross-section increased from small size to medium size and then to large size, and the nominal shear strengths were 5.07, 4.79, and 4.42 MPa, respectively. For beams of the same size, the nominal shear strength increased significantly with increasing prestress level. The higher the prestress level, the more pronounced the strength enhancement, and the increase remained relatively stable. For the small-sized beams, the prestress level increased from 0 to 0.228 and 0.431, and the nominal shear strength increased by 14.81% and 34.13%, respectively; for medium-sized beams: the prestress level increased from 0 to 0.228 and 0.431, and the nominal shear strength increased by 14.50% and 37.80%, respectively; for large-sized beams: the prestress level increased from 0 to 0.228 and 0.431, and the nominal shear strength increased by 22.05% and 44.26%, respectively. The main reason is that the application of prestress can effectively restrain the initiation and propagation of shear cracks in the beam, reduce the shear damage in the section, and improve the overall shear resistance of the section. The large-sized beams are more strongly affected by the size effect and have relatively weaker shear performance. The strengthening effect of prestress is more prominent, and the improvement is greater than that of small-sized beams. The nominal shear strength of prestressed recycled concrete beams is jointly governed by size and prestress level—an increase in size leads to a decrease in nominal shear strength, whereas an increase in prestress level significantly improves the nominal shear strength, and the strengthening effect of prestress on large-sized beams is more obvious.

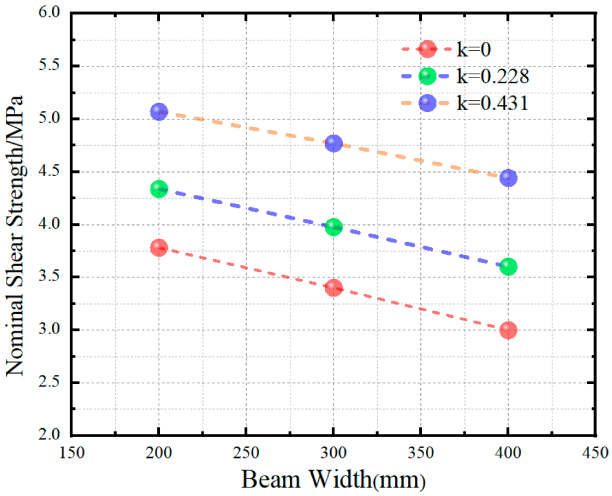

Figure 7. Nominal shear strength of prestressed RAC beams with different prestress levels.

Bažant's Size Effect Law (SEL) [13] describes the changing strength law of quasi-brittle structural members with geometric dimensions. For small-section beams, internal stress can be fully redistributed prior to failure, leading to ductile failure modes. As the beam section size increases, the structure gradually presents brittle failure characteristics, accompanied by a decline in overall nominal shear strength. The simulation results of this study are consistent with the above law. Under the non-prestressed condition k = 0, when the beam depth rises from 350 mm to 700 mm, the nominal shear strength drops from 3.78 MPa by 19%. Prestress can restrain the growth of internal cracks and local damage in beams and mitigate the adverse influence induced by member size. Large-sized beams suffer more severe negative impacts from the size effect, so prestress delivers a more obvious

improvement in shear performance. In this research, the nominal shear strength of large-sized beams rises by 44.26%, versus 34.13% for small-sized beams, which fully proves that prestress can effectively weaken the shear size effect of recycled concrete beams.

4. Analysis of Shear Performance and Size Effect of Prestressed RAC Beams Under Different Strain Rates

4.1. Failure Modes Under Different Strain Rates

By varying the dynamic loading rate, the shear failure modes and size effects of beams with different cross-sectional dimensions under different strain rates were studied. The simulated reinforcement ratio was 1.03%, the stirrup ratio was 0.141%, the shear span-to-depth ratio was 2.1, the prestress level was 0.228, the recycled aggregate replacement ratio was 30%, and the strain rates were 10^{-5}/s, 10^{-3}/s, 10^{-1}/s, 1/s, 10/s. The cross-sectional dimensions were 200 mm × 350 mm, 300 mm × 525 mm, and 400 mm × 700 mm, with a total of 15 prestressed recycled concrete beams. The relevant geometric parameters of the beams are shown in Table 4.

Table 4. Geometric model parameters of prestressed RAC beams under different strain rate loading conditions.

Test Specimen Name	Cross-Sectional Dimension $b \times h$/mm	Beam Length/mm	Replacement Rate r%	Shear Span-to-Depth Ratio λ	Prestress Level k	Strain Rate $\dot{\varepsilon}$/s
DRAC-Sd1	200 × 350	3200	30	2.1	0.228	10^{-5}
DRAC-Sd2	200 × 350	3200	30	2.1	0.228	10^{-3}
DRAC-Sd3	200 × 350	3200	30	2.1	0.228	10^{-1}
DRAC-Sd4	200 × 350	3200	30	2.1	0.228	1
DRAC-Sd5	200 × 350	3200	30	2.1	0.228	10
DRAC-Md1	300 × 525	4200	30	2.1	0.228	10^{-5}
DRAC-Md2	300 × 525	4200	30	2.1	0.228	10^{-3}
DRAC-Md3	300 × 525	4200	30	2.1	0.228	10^{-1}
DRAC-Md4	300 × 525	4200	30	2.1	0.228	1
DRAC-Md5	300 × 525	4200	30	2.1	0.228	10
DRAC-Ld1	400 × 700	6200	30	2.1	0.228	10^{-5}
DRAC-Ld2	400 × 700	6200	30	2.1	0.228	10^{-3}
DRAC-Ld3	400 × 700	6200	30	2.1	0.228	10^{-1}
DRAC-Ld4	400 × 700	6200	30	2.1	0.228	1
DRAC-Ld5	400 × 700	6200	30	2.1	0.228	10

As shown in Figure 8, under dynamic loading conditions, the sectional dimensions significantly affect the crack distribution, crack propagation rate, and final failure mode of prestressed recycled concrete beams. Small-sized (200 mm × 350 mm), medium-sized (300 mm × 525 mm), and large-sized (400 mm × 700 mm) beams were selected for comparison of failure characteristics under different strain rates. The results show that as the section size increases, the failure mode of the beam exhibits a pronounced size effect: for small-sized beams, the number of cracks is relatively larger, the crack distribution is concentrated, the critical inclined crack is shorter and wider, the crack propagation path is shorter and energy dissipation is faster under dynamic loading, and the failure is mainly characterized by local shear-compression crushing; for medium-sized beams, the number of cracks decreases, the main inclined crack extends more clearly, the crack development rate is moderate, the failure mode is between shear and bending shear, and the dynamic response is relatively stable; for large-sized beams, the section stiffness significantly increases, the number of cracks decreases, the critical inclined crack is longer and more extended,

the crack expansion path is prolonged, the internal weak surface increases under dynamic loading, the energy dissipation efficiency is reduced, the nominal shear strength decreases, the inclined crack is more likely to propagate steadily through the beam and the overall failure shows more pronounced brittleness, the crushing area is distributed longer along the shear span direction, and the failure range is larger. Under the same section size, increasing the strain rate will accelerate the crack propagation, amplify the brittle failure trend, and the large-sized beam is more sensitive to the strain rate, with more rapid crack development and more sudden failure under high strain rates. From the mechanism perspective, the size dependence of concrete quasi-brittle materials is more significant under dynamic loading. Large-sized components have a higher probability of internal defects and more unstable crack expansion, while the prestressed prestress-induced compressive stress field can, to some extent, inhibit crack development and delay the brittle increase trend caused by the size effect, but it cannot completely eliminate the inherent influence of section size on the failure mode.

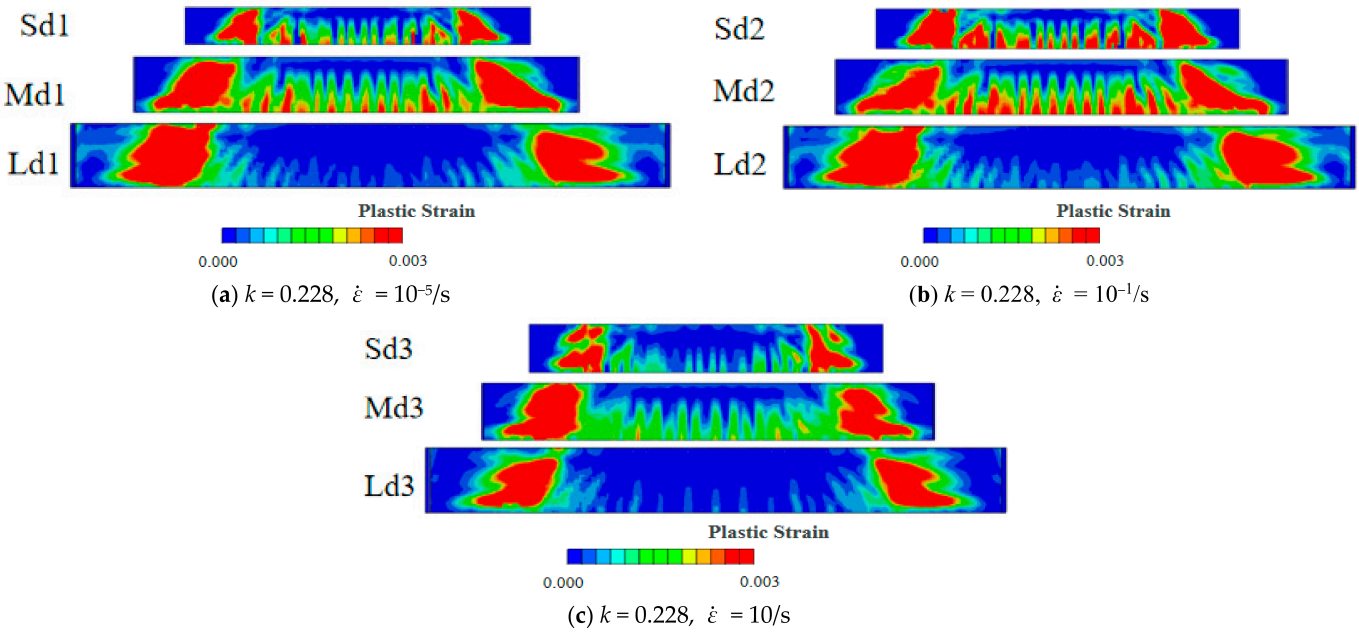

(**a**) $k = 0.228$, $\dot{\varepsilon} = 10^{-5}$/s (**b**) $k = 0.228$, $\dot{\varepsilon} = 10^{-1}$/s

(**c**) $k = 0.228$, $\dot{\varepsilon} = 10$/s

Figure 8. Failure modes of prestressed RAC beams under different strain rates.

4.2. Load–Displacement Curves at Different Strain Rates

As shown in Figure 9, under the conditions of 30% replacement rate of recycled aggregates, prestress force of 0.228, and a shear span ratio of 2.1, dynamic loading simulations were conducted on small-sized (200 mm × 350 mm), medium-sized (300 mm × 525 mm), and large-sized (400 mm × 700 mm) prestressed recycled concrete beams. The load–displacement curves and ultimate shear-bearing capacities under three loading rates (10^{-5}/s, 10^{-1}/s, 10/s) were compared. At the loading rate of 10^{-5}/s, the section size increased from small to medium and then to large, and the ultimate shear-bearing capacities were 260.18, 568.52, and 897.30 kN, respectively. At the loading rate of 10^{-1}/s, the ultimate shear-bearing capacities were 294.09, 644.97, and 1053.93 kN, respectively. The bearing capacities of beams of all sizes increased significantly under the high-strain-rate dynamic loading, and the growth trend remained stable. At the loading rate of 10/s, the dynamic strengthening effect was the most significant, and the ultimate shear-bearing capacities were 332.47, 748.73, and 1238.17 kN, respectively. The high strain rate had a significant strength enhancement effect for beams of all sizes. Under the same section size and different loading rates, when the loading rate of the small-sized beam increased from 10^{-5}/s to 10/s, the bearing

capacity increased from 260.18 kN to 332.47 kN, with an increase of 27.79%; for the medium-sized beam, the bearing capacity increased from 568.52 kN to 748.73 kN, with an increase of 31.69%; for the large-sized beam, the bearing capacity increased from 897.30 kN to 1238.17 kN, with an increase of 37.99%. The results show that the section size plays a dominant role in controlling the dynamic shear-bearing capacity, and the ultimate bearing capacity shows a significant growth trend with the increase in section size. At the same time, the increase in loading rate can produce a significant strain-rate strengthening effect, and the bearing capacity continues to increase with the increase in loading rate.

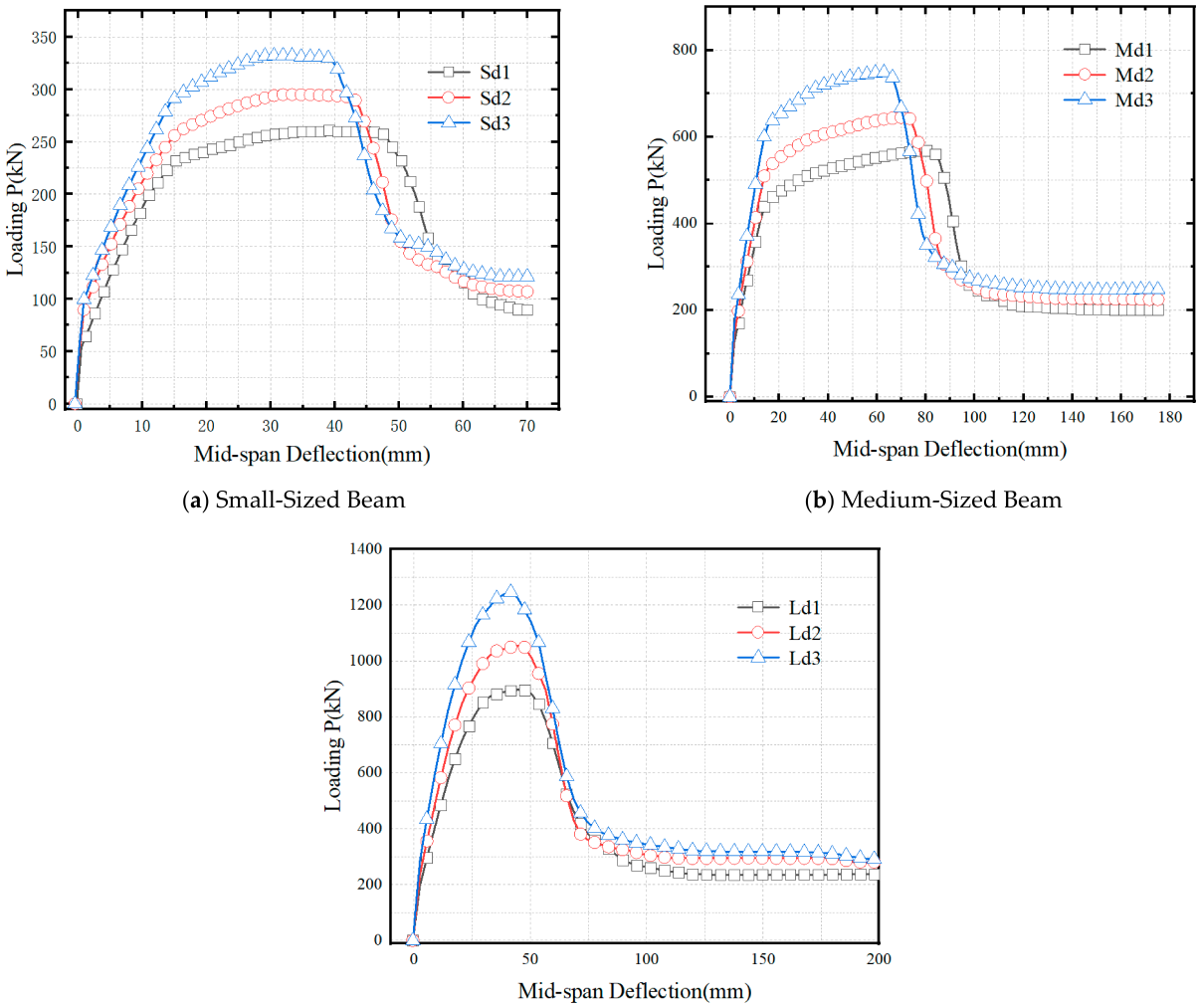

(**a**) Small-Sized Beam

(**b**) Medium-Sized Beam

(**c**) Large-Sized Beam

Figure 9. Load–displacement curves of prestressed RAC beams under different strain rates.

The amplitude of bearing capacity growth varies greatly among beams of different sizes: 37.99% for large-sized specimens, 31.69% for medium-sized specimens, and 27.79% for small-sized specimens. This phenomenon is closely linked to the material properties of recycled concrete and dynamic loading mechanisms. Compared with ordinary concrete, recycled concrete contains abundant micropores and weak interfacial transition zones (ITZs), and it is more sensitive to strain rate variation [31]. At low strain rates, internal defects and cracks have adequate time to develop gradually and expand along weak interfaces, forming tortuous crack paths and resulting in a gentle drop in bearing capacity. At high strain rates, rapid loading restrains progressive defect evolution. The compression between cracked planes strengthens aggregate interlock friction [29], together with the rise in the dynamic strength of reinforcement bars, significantly improving the shear capacity of

beams [27]. Large-sized beams possess more internal defects and longer crack propagation paths, so they obtain more remarkable comprehensive strengthening effects under dynamic loading and thus achieve the highest growth of shear-bearing capacity [30].

4.3. The Influence of Different Strain Rates on the Nominal Shear Strength of Beams

As shown in Figure 10, under the conditions of a 30% replacement rate of recycled aggregates, prestress force of 0.228, and a shear span ratio of 2.1, dynamic loading simulations were conducted on small-sized (200 mm × 350 mm), medium-sized (300 mm × 525 mm), and large-sized (400 mm × 700 mm) prestressed recycled concrete beams. The nominal shear strengths under three loading rates (10^{-5}/s, 10^{-1}/s, 10/s) were compared. At a loading rate of 10^{-5}/s, the nominal shear strengths of each size (small size, medium size, large size) were 4.33, 3.98, and 3.58 MPa, respectively; at a loading rate of 10^{-1}/s, the nominal shear strengths were 4.90, 4.52, and 4.21 MPa, respectively; at a loading rate of 10/s, the nominal shear strengths were 5.53, 5.25, and 4.95 MPa, respectively. From the data, it can be seen that the nominal shear strength of prestressed recycled concrete beams with the same cross-sectional size shows a significant upward trend as the strain rate increases, demonstrating a clear strain rate strengthening effect. Specifically, the total increase from low to high strain rate was 27.7% for the small-sized beam, 31.9% for the medium-scale beam, and 38.3% for the large-scale beam. This indicates that the larger the sectional size, the higher the sensitivity of the member to strain rate and the more pronounced the dynamic strengthening effect. Moreover, at a low strain rate (10^{-5}/s), the differences in nominal shear strength among beams of different sizes are relatively large, demonstrating a significant size effect. As the strain rate increases, these differences gradually decrease, and the size effect is markedly weakened. At a high strain rate (10/s), the three nominal shear strength curves tend to converge, indicating that increasing the loading rate can effectively suppress the rapid propagation and extension of cracks, reduce the mechanical performance differences caused by sectional size, and thus significantly alleviate the size effect of prestressed RAC beams.

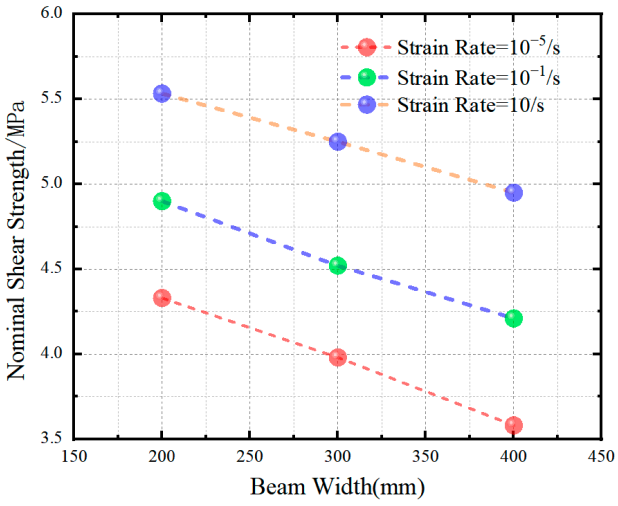

Figure 10. Nominal shear strength of prestressed RAC beams under different strain rates.

The elevation of strain rate can alleviate the size effect via two major mechanisms. First, recycled concrete achieves obvious dynamic strength enhancement under high strain rates, which lifts the crack propagation threshold and reduces the risk of unstable crack growth in large beams [27]. Second, the inertial confinement effect restrains free crack extension and narrows the disparity of crack development caused by different section dimensions [29]. Meanwhile, the precompressive stress generated by prestress can close

initial microcracks and enhance matrix compactness. It is inferred that such precompression produces a synergistic coupling effect with the high strain rate effect, further lowering the dimensional sensitivity of beams and weakening the size effect [23].

5. Theoretical Formulas for Shear Strength Size Effect

Bažant proposed a Size Effect Law suitable for concrete materials based on fracture mechanics theory:

$$\tau_u = V_0 / \sqrt{1 + \frac{D}{D_0}} \tag{17}$$

where τ_u is the nominal shear strength of the beam, V_0 and D_0 are empirical coefficients related to concrete, and D is the sectional height of the beam.

Combined with Equation (17), and to account for the effects of prestress level and strain rate on the size effect of RAC beams, this study proposes a modified Formula (5) introducing the shear strength enhancement coefficients γ and β:

$$\tau_u = V_0 / \sqrt{1 + \frac{D}{D_0}\gamma\beta} \tag{18}$$

5.1. Determination of Shear Strength Enhancement Coefficient γ

An increase in the prestress level reduces the size effect of prestressed RAC beams. Moreover, as the prestress level increases, the decreasing trend of nominal shear capacity with increasing sectional size becomes less pronounced. A linear function is adopted to describe the variation in the shear strength enhancement coefficient γ with the prestress level k:

$$\gamma = A + Bk \tag{19}$$

where coefficient B is determined through fitting (see Figure 11). The coefficient γ is obtained by taking the recycled aggregate concrete beam with a prestress level of 0 under quasi-static loading as the benchmark and calculating the ratio with other prestressed recycled aggregate concrete beams. The values of the shear strength enhancement coefficient γ are shown in Table 5. Figure 11 presents the variation trend of γ with the prestress level k and provides the expressions of γ for different sectional sizes. Finally, by establishing the relationship between coefficient B and the sectional dimension, a unified expression is fitted as:

$$\gamma = 1 + \left(0.5384 + 6.8257 \times 10^{-4} D\right)k \tag{20}$$

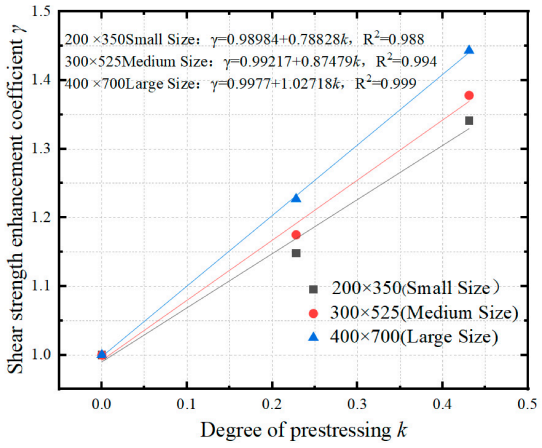

Figure 11. Determination of shear strength enhancement coefficient γ.

Table 5. Shear strength enhancement coefficient γ.

Specimen Name	γ	Specimen Name	γ	Specimen Name	γ
YRAC-200-30–2.1-0	1	YRAC-200-30–2.1-0.228	1.148	YRAC-200-30–2.1-0.431	1.341
YRAC-300-30–2.1-0	1	YRAC-300-30–2.1-0.228	1.145	YRAC-300-30–2.1-0.431	1.378
YRAC-400-30–2.1-0	1	YRAC-400-30–2.1-0.228	1.227	YRAC-400-30–2.1-0.431	1.443

5.2. Determination of Shear Strength Enhancement Coefficient β

Previous studies indicate that the strain rate has a significant effect on the ultimate shear capacity of prestressed RAC beams. As the strain rate increases, both the ultimate shear capacity and the nominal shear strength of prestressed RAC beams gradually increase, with the growth rate first increasing and then decreasing. Through multiple fitting attempts, it was found that using a "Logistic" function to represent the fitting curve between the strain rate $\dot{\varepsilon}$ and the enhancement coefficient β yields a smaller error, as shown in Equation (21):

$$\beta = I_2 + \frac{I_1 - I_2}{1 + (\frac{\dot{\varepsilon}}{\varepsilon_0})^p} \tag{21}$$

where is the strain rate. The coefficients I_1, I_2, ε_0 and p are determined through nonlinear fitting (see Figure 12). The coefficient is obtained by taking the prestressed RAC beam under quasi-static loading as the benchmark and calculating the ratio with the prestressed RAC beam under dynamic loading. The values of the shear strength enhancement coefficient are shown in Table 6. Finally, by establishing the relationship between the coefficients and the sectional size D, a unified expression is fitted as shown in Equation (22).

$$\beta = (1.199 + 3.7757 \times 10^{-4} D) + \frac{(1.00289 + 7.17429 \times 10^{-7} D) - (1.199 + 3.7757 \times 10^{-4} D)}{1 + (\frac{\dot{\varepsilon}}{0.21261 - 4.04286 \times 10^{-5} D})^{0.44877 - 6.38 \times 10^{-5} D}} \tag{22}$$

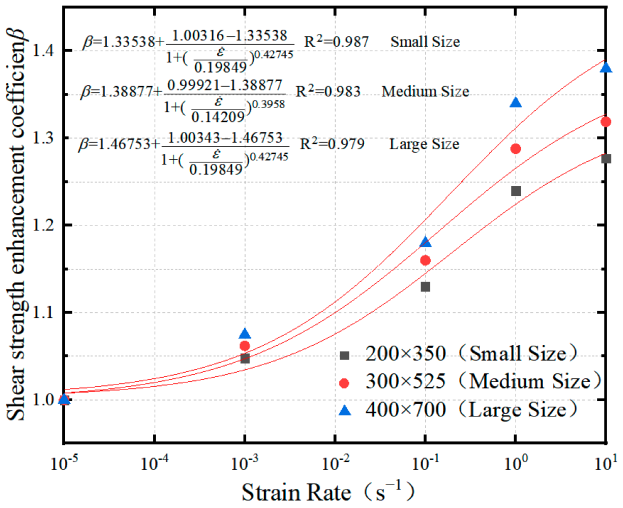

Figure 12. Determination of shear strength enhancement coefficient β.

Table 6. Shear strength enhancement coefficient β.

Specimen Name	β	Specimen Name	β	Specimen Name	β	Specimen Name	β	Specimen Name	β
YRAC-200-10^{-5}	1	YRAC-200-10^{-3}	1.052	YRAC-200-10^{-1}	1.132	YRAC-200-1	1.205	YRAC-200-10	1.277
YRAC-300-10^{-5}	1	YRAC-300-10^{-3}	1.059	YRAC-300-10^{-1}	1.144	YRAC-300-1	1.240	YRAC-300-10	1.319
YRAC-400-10^{-5}	1	YRAC-400-10^{-3}	1.068	YRAC-400-10^{-1}	1.175	YRAC-400-1	1.270	YRAC-400-10	1.380

5.3. Validation of Formula Effectiveness

Since there is currently a lack of published experimental studies on RAC beams that take prestress level, strain rate, and sectional size as parameters, this study established additional models for validation. Specifically, three prestressed RAC beams with a sectional size of 250 mm × 438 mm were modeled under a dynamic strain rate of 10^{-5}/s, with a longitudinal reinforcement ratio of 1.03%, a stirrup ratio of 0.141%, a shear span-to-depth ratio of 2.1, prestress levels of 0, 0.228, and 0.431, and a recycled aggregate replacement ratio of 30%. In addition, beams with a prestress level of 0.228 and sectional sizes of 250 mm × 450 mm and 350 mm × 600 mm were modeled under dynamic loading at strain rates of 10^{-5}/s, 10^{-3}/s, 10^{-1}/s, 1/s and 10/s, resulting in a total of 12 beams. The relevant data are listed in Table 7. These data were substituted into Equation (18) for validation, and the results are shown in Table 8.

Table 7. Model parameters for extended analysis of prestressed RAC beams.

Specimen Name	Cross-Sectional Size $b \times h$/mm	Replacement Ratio r%	Shear Span-to-Depth Ratio λ	Prestress Level k	Strain Rate $\dot{\varepsilon}$/s
XRAC1	250× 450	30	2.1	0	10^{-5}
XRAC2	250 × 450	30	2.1	0.228	10^{-5}
XRAC3	250 × 450	30	2.1	0.431	10^{-5}
XRAC4	250 × 450	30	2.1	0.228	10^{-3}
XRAC5	250 × 450	30	2.1	0.228	10^{-1}
XRAC6	250 × 450	30	2.1	0.228	1
XRAC7	250 × 450	30	2.1	0.228	10
VRAC1	350 × 600	30	2.1	0.228	10^{-5}
VRAC2	350 × 600	30	2.1	0.228	10^{-3}
VRAC3	350 × 600	30	2.1	0.228	10^{-1}
VRAC4	350 × 600	30	2.1	0.228	1
VRAC5	350 × 600	30	2.1	0.228	10

Table 8. Comparison between simulation values and predicted values from the proposed method.

Beam Height (mm)	Prestress Level k	Strain Rate $\dot{\varepsilon}$/s	Simulated Value (MPa)	Calculation γ	Calculation β	Predicted Value (MPa)	Relative Error (%)
450	0	10^{-5}	3.69	1.000	1.000	3.60	2.53
450	0.228	10^{-5}	4.27	1.193	1.000	4.29	−0.39
450	0.431	10^{-5}	4.91	1.364	1.000	4.91	0.00
450	0.228	10^{-3}	4.76	1.204	1.056	4.53	5.14
450	0.228	10^{-1}	4.92	1.385	1.139	4.89	0.52
450	0.228	1	5.26	1.000	1.225	5.26	0.00
450	0.228	10	5.60	1.232	1.301	5.58	0.40
600	0.228	10^{-5}	4.08	1.218	1.000	4.09	−0.29
600	0.228	10^{-3}	4.47	1.218	1.063	4.35	2.82
600	0.228	10^{-1}	4.87	1.218	1.157	4.74	2.73
600	0.228	1	5.43	1.218	1.253	5.13	5.90
600	0.228	10	5.79	1.218	1.345	5.51	5.14

Note: The average error between the predicted values of the modified formula and the simulated values is only 2.61%, with the maximum error controlled within 6%. This indicates that the proposed modified formula containing the enhancement coefficients γ and β can accurately reflect the results calculated by the finite element model. The extended validation cases adopted in this study are still derived from numerical samples generated within the unified modeling framework of the present work, rather than third-party experimental data or a completely independent numerical dataset. Therefore, the proposed model does not possess unconditional predictive capability for extrapolation to other loading conditions, materials, or structural forms. Based on the experimental parameters considered in this study, the strict scope of applicability of the proposed equation is defined as follows: replacement ratio of recycled coarse aggregate of 30%, shear span-to-depth ratio of 2.1, prestress level ($k \leq 0.431$), strain rate range of 10^{-5}/s~10/s, and beam sectional height of 350–700 mm. When the parameters exceed the above ranges, the coefficients must be recalibrated.

6. Conclusions

This paper is based on the 3D five-phase meso-scale numerical model. Within the parameter scope with a fixed replacement ratio of recycled coarse aggregate of 30%, s shear span-to-depth ratio of 2.1, prestress level ≤ 0.431, strain rate ranging from 10^{-5}/s to 10/s, and cross-sectional height of 350–700 mm, numerical analysis is carried out on the shear mechanical properties and specimen size effect of prestressed recycled aggregate concrete (RAC) beams under dynamic loading. The conclusions obtained belong to exploratory numerical analysis results. The main observations are listed as follows:

1. The 3D five-phase meso-scale numerical model established in this paper can satisfactorily reflect the meso-scale heterogeneous characteristics of recycled aggregate concrete and the action mechanism of prestress. The simulated failure modes, crack development law and load–displacement curves are in good agreement with quasi-static test results, and the maximum error is less than 10%. Within the parameter range specified in this paper, the model can be adopted for numerical analysis on the dynamic shear mechanical properties of prestressed RAC beams.
2. Within the researched parameter range, raising the prestress level can significantly restrain the initiation and propagation of diagonal cracks, reduce the failure brittleness of members, and effectively weaken the shear size effect. As the prestress level rises from 0 to 0.431, the nominal shear strengths of small-sized and large-sized beams increase by 34.1% and 44.3%, respectively; the displacement ductility coefficient of large-sized beams grows from 1.65 to 2.92, presenting an obvious ductility improvement effect.
3. Within the researched parameter range, prestressed RAC beams exhibit an obvious specimen size effect in terms of nominal shear strength, and the nominal shear strength decreases with the increase in cross-sectional height. With the rise in loading strain rate, the shear-bearing capacity of members presents a comprehensive dynamic response formed by the coupling of material rate effect and structural inertia effect. As the strain rate increases from 10^{-5}/s to 10/s, the nominal shear strengths of small-sized, medium-sized and large-sized beams rise by 27.8%, 31.7% and 38.0%, respectively; the larger the section size, the higher the dynamic response sensitivity of prestressed RAC beams. High strain rate can reduce the difference in shear mechanical properties of members with various sizes and further mitigate the size effect.
4. Based on Bažant's Size Effect Law (SEL), a modified formula is developed by introducing the prestress enhancement coefficient γ and strain rate enhancement coefficient β. The formula achieves a favorable fitting effect merely within the parameter range studied in this paper; the average error between predicted values and simulated values of the formula is 2.61%, and the maximum error is less than 6%. Nevertheless, due to the lack of corresponding dynamic test data for verification, the formula proposed in this paper is only applicable to calibrated correlation within the studied parameter space rather than a widely applicable prediction model, and its predictability under other materials, geometric configurations and loading conditions requires further verification.

Author Contributions: Conceptualization, C.L.; methodology, C.L. and F.A.; software, C.L. and Z.T.; validation, C.L.; formal analysis, C.L., B.H. and W.N.; investigation, X.L.; data curation, C.L., X.L. and Z.T.; writing—original draft, C.L.; writing–review and editing, C.L., X.L., B.H., W.N. and F.A.; visualization, C.L. All authors have read and agreed to the published version of the manuscript.

Funding: This work was supported by the Kashi University Research Startup Funding Project (Grant No. GCC2025ZK-021), university-level research project (cultivation) (2025) 21022, and Research on Key Technologies of Intelligent Design and Green Sustainable Development of Prefabricated Buildings (Grant No. 2025B04050-001).

Data Availability Statement: The original contributions presented in this study are included in the article. Further inquiries can be directed to the corresponding author.

Conflicts of Interest: The authors declare no conflicts of interest.

References

1. Wang, B.; Yan, L.; Fu, Q.; Kasal, B. A comprehensive review on recycled aggregate and recycled aggregate concrete. *Resour. Conserv. Recycl.* **2021**, *171*, 105565. [CrossRef]
2. Verian, K.P.; Ashraf, W.; Cao, Y. Properties of recycled concrete aggregate and their influence in new concrete production. *Resour. Conserv. Recycl.* **2018**, *133*, 30–49. [CrossRef]
3. Limbachiya, M.C.; Leelawat, T.; Dhir, R.K. Use of recycled concrete aggregate in high-strength concrete. *Mater. Struct.* **2000**, *33*, 574–580. [CrossRef]
4. Xiao, J.; Li, J.; Sun, Z.; Hao, X. Study on compressive strength of recycled concrete. *J. Tongji Univ. (Nat. Sci. Ed.)* **2004**, *12*, 1558–1561. [CrossRef]
5. Pacheco, J.; De Brito, J.; Chastre, C.; Evangelista, L. Experimental investigation on the variability of the main mechanical properties of concrete produced with coarse recycled concrete aggregates. *Constr. Build. Mater.* **2019**, *201*, 110–120. [CrossRef]
6. Xu, Z.; Shi, J. performance analysis and evaluation of recycled aggregate and recycled aggregate concrete. *Concrete* **2006**, *7*, 41–46. [CrossRef]
7. Wang, Z.; Wang, S.; Weng, G. Experimental study on mechanical properties of recycled concrete with different coarse aggregate replacement rates. *J. Zhengzhou Univ. (Eng. Ed.)* **2012**, *33*, 32–35. [CrossRef]
8. Kristensen, C.; Hoang, L.C.; Sørensen, J.H.; Hansen, L.Z.P.; Fischer, G.D. Mechanical Properties of Structural Concrete with Recycled Concrete Aggregates at High Replacement Ratios. *Nord. Concr. Res.* **2026**, *73*, 57–81. [CrossRef]
9. Du, C. Experimental study on flexural behavior of recycled aggregate concrete beams. *Concrete* **2012**, *3*, 77–80. [CrossRef]
10. Fathifazl, G.; Razaqpur, A.G.; Isgor, O.B.; Abbas, A.; Fournier, B.; Foo, S. Shear strength of reinforced recycled concrete beams with stirrups. *Mag. Concr. Res.* **2010**, *62*, 685–699. [CrossRef]
11. Zhao, J.; Yang, Q.; Zhang, Y.; Wang, X.; Lu, C.; Liang, C.; Sun, B. Experimental study on size effect of shear performance of recycled concrete beams without web reinforcement. *Concrete* **2018**, *6*, 39–42. [CrossRef]
12. Xiao, J.; Lan, Y. Experimental study on shear behavior of recycled aggregate concrete beams. *Struct. Eng.* **2004**, *6*, 54–58+53. [CrossRef]
13. Bazoant, Z.P. Size effect in blunt fracture: Concrete, rock, metal. *J. Eng. Mech.* **1984**, *110*, 518–535. [CrossRef]
14. Bazant, Z.P.; Planas, J. *Fracture and Size Effect in Concrete and Other Quasibrittle Materials*; Routledge: Boca Raton, FL, USA, 2019. Available online: https://api.taylorfrancis.com/content/books/mono/download?identifierName=doi&identifierValue=10.1201/9780203756799&type=googlepdf (accessed on 17 April 2026).
15. Bazant, Z.P.; Kazemi, M.T. Size effect on diagonal shear failure of beams without stirrups. *ACI Struct. J.* **1991**, *88*, 268–276. [CrossRef]
16. Bažant, Z.P.; Yu, Q. Designing against size effect on shear strength of reinforced concrete beams without stirrups: I. Formulation. *J. Struct. Eng.* **2005**, *131*, 1877–1885. [CrossRef]
17. Syroka-Korol, E.; Tejchman, J. Experimental investigations of size effect in reinforced concrete beams failing by shear. *Eng. Struct.* **2014**, *58*, 63–78. [CrossRef]
18. Jin, L.; Wang, T.; Du, X.; Xia, H. Study on shear failure and size effect law of reinforced concrete cantilever beam. *Eng. Mech.* **2020**, *37*, 53–62. [CrossRef]
19. Jin, L.; Wang, T.; Du, X. Theoretical study on shear strength and size effect of RC cantilever beam without web reinforcement. *J. Comput. Mech.* **2020**, *37*, 396–404. [CrossRef]
20. Liu, C.; Zhou, G.; Wang, H.; Wang, Y. Theoretical Research on the Shear Mechanical Properties and Size Effect of Recycled Concrete Beams Without Stirrups. *Buildings* **2025**, *15*, 1737. [CrossRef]
21. Park, J.Y.; Krauthammer, T. Development of an LEFM dynamic crack criterion for correlated size and rate effects in concrete beams. *Int. J. Impact Eng.* **2009**, *36*, 92–97. [CrossRef]
22. Jia, J.; Yao, D.; Yu, F. Experimental study on shear behavior of prestressed steel reinforced ultra-high strength concrete beams under concentrated load. *J. Build. Struct.* **2013**, *34*, 112–120. [CrossRef]
23. Brandes, M.R.; Kurama, Y.C. Behavior of shear-critical prestressed concrete beams with recycled concrete aggregates under ultimate loads. *Eng. Struct.* **2018**, *165*, 237–246. [CrossRef]

24. Jafari, A.; Shahmansouri, A.A.; Pourshamsian, S.; Bengar, H.A.; Zhou, Y. Post-tensioned coupling beams: Mechanics, cyclic response, and damage evaluation. *Soil Dyn. Earthq. Eng.* **2025**, *188*, 109082. [CrossRef]
25. Abdul-Rahman, R.; Saletti, D.; Forquin, P. Experimental study of the static and dynamic behavior of pre-stressed concrete subjected to shear loading. *Eng. Struct.* **2021**, *234*, 111865. [CrossRef]
26. Fan, H.; Yu, H.; Ma, H. Dynamic increase factor (DIF) of concrete with SHPB tests: Review and systematic analysis. *J. Build. Eng.* **2023**, *79*, 107666. [CrossRef]
27. Jin, L.; Yu, W.; Du, X.; Zhang, S.; Yang, W.; Li, D. Size effect of dynamic compressive strength of concrete based on mesoscopic simulation. *Eng. Mech.* **2019**, *36*, 50–61. [CrossRef]
28. Jin, L.; Li, J.; Yu, W.; Du, X. Microscopic analysis of the influence of structural size on the biaxial dynamic failure behavior of concrete. *Vib. Shock* **2022**, *41*, 1–9. [CrossRef]
29. Işık, L.; Turan, O.T.; Ataoglu, S.; Dönmez, A.A. Effects of strain rate and size on concrete under shear using push-off tests. *J. Mater. Civ. Eng.* **2023**, *35*, 04023168. [CrossRef]
30. Jin, L.; Zhang, J.; Li, D.; Du, X. Meso-scale study on dynamic shear behavior and size effect of reinforced concrete beams. *J. Vib. Shock* **2023**, *42*, 194–205. [CrossRef]
31. Li, L. Dynamic Mechanical Behavior of Recycled Aggregate Concrete. Ph.D. Thesis, The Hong Kong Polytechnic University, Hong Kong, China, 2018. Available online: https://theses.lib.polyu.edu.hk/handle/200/9515 (accessed on 18 April 2026).
32. Naderi, S.; Zhang, M. Meso-scale modelling of static and dynamic tensile fracture of concrete accounting for real-shape aggregates. *Cem. Concr. Compos.* **2021**, *116*, 103889. [CrossRef]
33. Liu, C.; Gao, Y.; Luan, K.; Su, J.; Lin, Y. Size effect on dynamic compressive failure mode and mechanical properties of recycled concrete. *Struct. Concr.* **2023**, *24*, 6370–6391. [CrossRef]
34. Zhuo, J.; Zhang, Y.; Ma, M.; Zhang, Y.; Zheng, Y. Uniaxial compression failure and size effect of recycled aggregate concrete based on meso-simulation analysis. *Materials* **2022**, *15*, 5710. [CrossRef] [PubMed]
35. Liu, C.; Qin, J.; Akbar, A. Study on flexural mechanical properties and size effect of recycled coarse aggregate concrete beams based on 3D mesoscopic simulation. *Struct. Concr.* **2025**, *26*, 7489–7508. [CrossRef]
36. Zhang, Z. Analysis of Meso-Mechanical Model of Recycled Concrete Based on Random Aggregate. Master's Thesis, Huazhong University of Science and Technology, Wuhan, China, 2020. [CrossRef]
37. Zhou, X.Q.; Hao, H. Modelling of compressive behaviour of concrete-like materials at high strain rate. *Int. J. Solids Struct.* **2008**, *45*, 4648–4661. [CrossRef]
38. Chen, Q.; Zhang, J.; Wang, Z.; Zhao, T.; Wang, Z. A review of the interfacial transition zones in concrete: Identification, physical characteristics, and mechanical properties. *Eng. Fract. Mech.* **2024**, *300*, 109979. [CrossRef]
39. Chen, Y.; Feng, J.; Zhu, T.; Li, F. Toughening mechanism and meso-scale fracture simulation of concrete with different aggregate volume fractions. *Acta Mater. Compos. Sin.* **2022**, *39*, 4972–4987. [CrossRef]
40. Liu, Q.; Cheng, A.; Sun, C.; Chen, K.; Wang, Y.; Li, W. Effects of aggregate's type and orientation on stress concentration and crack propagation of modeled concrete applied a shear force. *J. Build. Eng.* **2024**, *95*, 110340.
41. *GB 50010-2010*; Code for Design of Concrete Structures. China Architecture & Building Press: Beijing, China, 2010; pp. 227–228.
42. Yue, Q.; Wang, L.; Liu, F.; An, X. numerical study of recycled concrete failure based on real mesoscopic model. *J. Build. Mater.* **2016**, *19*, 221–228. [CrossRef]
43. Bažant, Z.P.; Oh, B.H. Crack band theory for fracture of concrete. *Mater. Struct.* **1983**, *16*, 155–177. [CrossRef]
44. Wu, Z.; Zhang, J.; Fang, Q.; Yu, H.; Ma, H. Mesoscopic modelling of concrete material under static and dynamic loadings: A review. *Constr. Build. Mater.* **2021**, *278*, 122419. [CrossRef]
45. Xu, W.; Zhang, C. Mechanical Behavior Characteristics of Sandstone and Constitutive Models of Energy Damage Under Different Strain Rates. *Appl. Sci.* **2025**, *15*, 7954. [CrossRef]
46. Al-Bukhaiti, K.; Yanhui, L.; Shichun, Z.; Daguang, H. Investigating the effectiveness of CFRP strengthening in improving the impact performance of RC members. *Structures* **2024**, *60*, 105841. [CrossRef]
47. Zhang, W.H.; Liu, P.Y.; Lü, Y.J. Research progress on dynamic mechanical properties of ultra-high performance concrete. *Mater. Rev.* **2019**, *33*, 3257–3271. [CrossRef]
48. Hu, Y. Experimental Study on Shear Behavior of Assembled Monolithic Prestressed Concrete beams. Master's Thesis, Guangxi University, Nanning, China, 2018. [CrossRef]

Disclaimer/Publisher's Note: The statements, opinions and data contained in all publications are solely those of the individual author(s) and contributor(s) and not of MDPI and/or the editor(s). MDPI and/or the editor(s) disclaim responsibility for any injury to people or property resulting from any ideas, methods, instructions or products referred to in the content.